Mapping Soil Rutting Probability across Cut Blocks using LiDAR-derived Depth to Water and Topographic Position Index Layers

Elizabeth White

BSc Environment and Natural Resources Honor's Report

Dr. Paul Arp, Supervisor

Faculty of Forestry and Environmental Management

University of New Brunswick

April 2022

Acknowledgments

I would like to thank Dr. Arp for his support, patience, and guidance throughout the duration of this project and for inspiring me to follow a path of continued learning. Additionally, I would like to thank Daniel Snow, Shirazum Munira and Jae Ogilvie for their support and help with the analysis of the study area.

Abstract

Soil rutting is the result of poor trafficability when soil moisture conditions render soil unable to resist compaction and displacement. Rutting can have deleterious impacts to the ecology of the affected area, with impacts on water flow and retention, site regeneration and soil erosion. Additional effects include the increased cost for maintenance of forest machinery and lowered efficiency in operations. The aim of this analysis was to determine the extent to which terrain and soil moisture indices could predict the probability of rutting. This was done via imagery analysis of a 250,000-ha study area located in central New Brunswick, Canada. Points were placed on instances of rutting and non-rutting throughout 400 cut blocks and delineated as 1 for rutting occurrences and 0 for non-rutting occurrences. Following this, raster layers were created for the slope in percent, sinks, Topographic Wetness Index, Topographic Position Index, Depth to Water 4ha, flow accumulation and direction all derived from the available provincial LiDAR data from the GeoNB database. The Multivariate extraction tool was used to extract data layer information from underneath each point, which was then analyzed in Statview to formulate a logistic regression model. The Topographic Position Index and Depth to Water 4ha were deemed as the best predictor variables for rutting within the study area, with a best-fitted predicted overall percentage of 84.93% for both observed and predicted incidences of rutting and non-rutting.

Introduction

Soil rutting is the result of poor soil trafficability and is caused by the forestry industry and military operations when soil moisture levels vary upwards from the soil retaining field capacity towards soil saturation. This primarily occurs due to combined wet weather conditions and poor soil drainage in depressions, along streams and low-lying land next to wetlands, lakes, ponds, and shores. For these conditions and locations, soils do not have sufficient strength to resist soil compaction and displacement (Nugent et al., 2003; Labelle and Jaeger, 2011; Duncker et al., 2012; Goutal et al., 2013; Sirén et al., 2013; Kauppinen et al., 2016; Riggert et al., 2016; Launiainen et al., 2019 as cited in Salmivaara et al., 2021, Pundir & Garg, 2021).

Heavy traffic–induced soil compaction reduces soil water infiltration, percolation, and aeration, while increasing soil density and causing root damage (Cambi et al. 2018a, 2018b; Jansson and Wasterlund 1999; Mariotti et al. 2020; Sirén et al. 2013; Solgi et al. 2019; Sugai et al. 2020; Batey 2009; Lee et al. 2020 as cited in Marra et al., 2021). Recovery from rutting generally varies from ephemeral on sandy soils, to long-lasting on loamy to clayey soils (Bottinelli et al. 2014; Jourgholami et al. 2020 as cited in Marra et al., 2021).

After formation, ruts may block or facilitate the flow of water across affected areas (Marion and Olive 2006 as cited in Campbell et al. 2013). Increased water flow enhances soil erosion and hence sediment transfer and sediment build-up in waterways, lakes, and shores (Morgan et al., 1983). Poor trafficability resulting in ruts also leads to inefficiencies in forest operations such as wood harvesting, wood retrieval, and follow-up site preparations. These inefficiencies refer to (i) machines becoming stuck in the soil, which invariably leads to further soil compaction and displacement, (ii) increased machine maintenance costs, and (iii) reduced abilities in maintaining the standards of imposed best-management practices and certification protocols (Marchi et al. 2018 as cited in Marra et al., 2021; Ares et al. 2005; as cited in Ezzati et al., 2012, Salmivaara et al., 2021; Suvinen, 2006 as cited in Niemi et al., 2017).

While forest harvest operations are best done when soils are frozen, there is a concern that sustained periods of frozen soils are becoming shorter due to increasing winter warming and incidences sporadic mid-winter warm-weather rainfalls (Lehtonen et al., 2019).

Trafficability is largely dependent on-site factors such as soil type, slope or topography, land use and soil moisture content (Pundir & Garg, 2021). Since soil moisture conditions generally vary from ridgetops to depressions, it has become possible to approximate these variations through elevation-derived terrain and soil moisture wetness indices such as the Terrain Wetness Index (TWI) (Beven and Kirkby, 1979 as cited in Mattila & Tokola, 2019), Topographic Position Index (TPI), and the cartographic Depth-To-Water Index (DTW) (Murphy et al., 2009). The derivation of these indices has been facilitated through the increasing availability of LiDAR-derived digital elevation models (DEMs) at 1 m resolution. The objective of this thesis is to demonstrate the extent to which these indices can be used to delineate where rut-inducing conditions across forested terrain likely exist. This is done by:

1. systematically marking where did and did not occur within-cut-block forest operations by inspecting high resolution surface images,
2. determining the extent to which these occurrences and non-occurrences could be captured by way of a logistic regression model using the LiDAR-DEM derived terrain variables TWI, TPI, DTW and slope in combination with soil type as predictor variables.

This was done by image and terrain analysis, inspecting approximately 400 cut blocks all located within a 250,000-ha wide area located in central New Brunswick (Figure 1).

Methodology

Study Area

The area of interest (AOI) falls within Sudbury, York and Northumberland counties of New Brunswick. This area is characterized as having average daily temperatures that range from -10 ºC to 19 ºC, and an average precipitation of 1100mm annually (Government of Canada: Environment and Natural Resources, 2021). The southernmost portion of the study area is located within the Saint John River watershed and the more northern region is located within the Miramichi river watershed, both of which are major river systems within the province and whose banks follow many urbanized areas including major cities.

The study area is comprised of softwood and hardwood mixed forests as well as several plots of farmland. Ownership across the selected area varied from crown land, private woodlots or land owned or managed by the JD Irving Limited Woodlands division and Acadia Forest Research Station. Forest harvest operations varied by harvesting methods, mainly referring to clear cutting and strip cutting.

Multiple image sources were used to obtain the highest resolution possible for this study area. The images from Google Earth were taken during varying time periods and over the course of several seasons and patched together to form the total aerial imagery. This resulted in portions of the study area having lower-resolution and occasional winter-time imagery. Thus, imagery was taken from additional sources such as the GeoNB enhanced imagery layer for the province. This imagery was of higher resolution and could supplement the areas of wintertime imagery. It was imperative to use the best possible imagery for this analysis as the rut-point placement was derived from this imagery to remove bias in the selection of rutting areas.

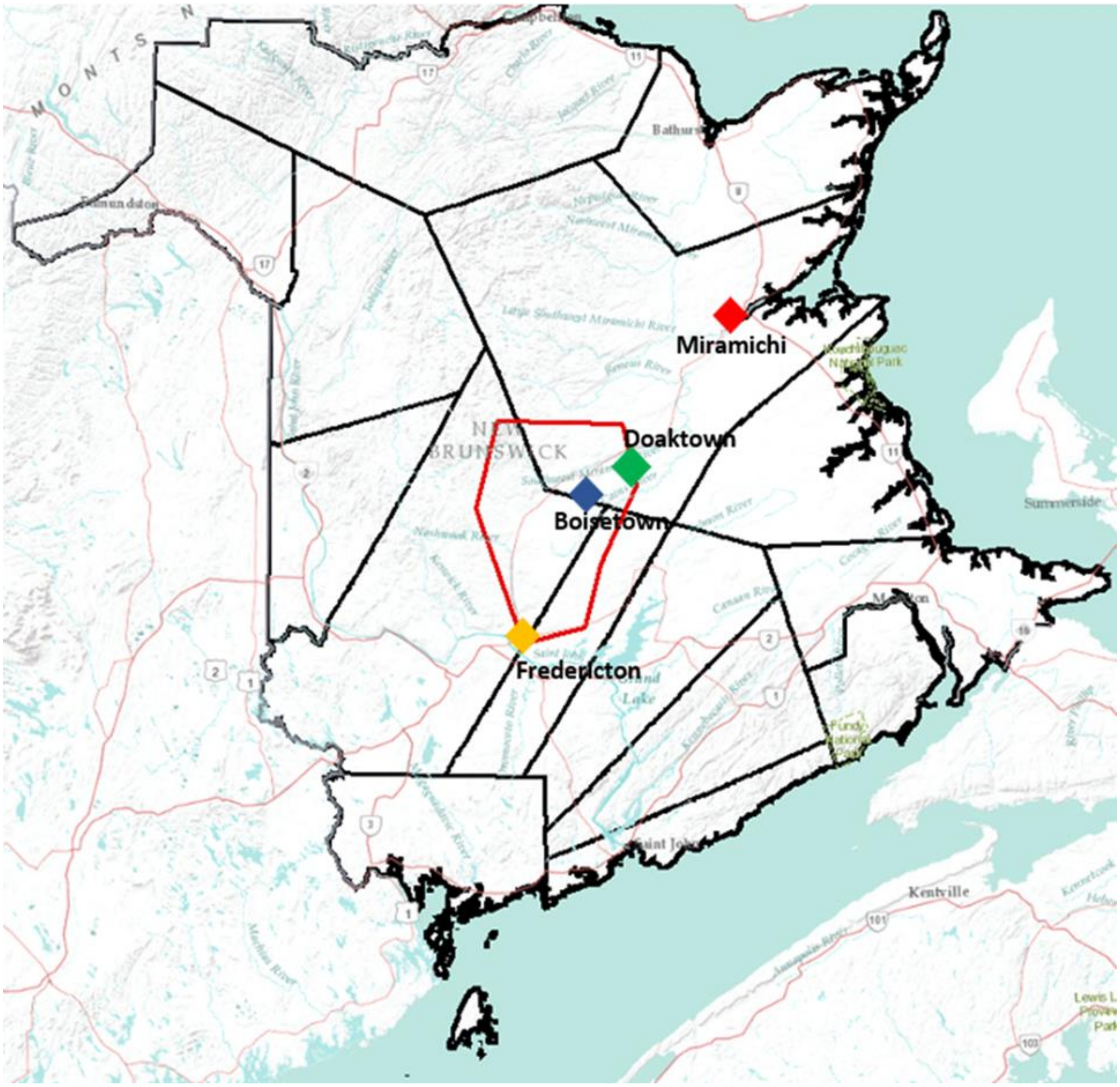

Figure 1. Map of the study area (red polygon) with nearby major cities as well as cities located with the study area indicated with the white text and coloured diamonds with the provincial counties outlined.

Imagery Analysis

Rutting within the blocks varied from absent to extensive by severity, as noted by inspecting high-resolution GeoNB, ESRI, Bing and 2000-2020 Historical Google Earth imageries. The resulting block by block examination across an estimated 400 cut blocks generated an ArcMap shapefile containing 2926 data points, marked 1 where clearly visible single-pass rutting occurred, and 0 where rutting was absent altogether. This marking was limited to locating 3 to 5 rut and non-rut locations within each cut block. The surface-generated cut block images at 0.05m cell size were compiled into a mosaic dataset after being georeferenced.

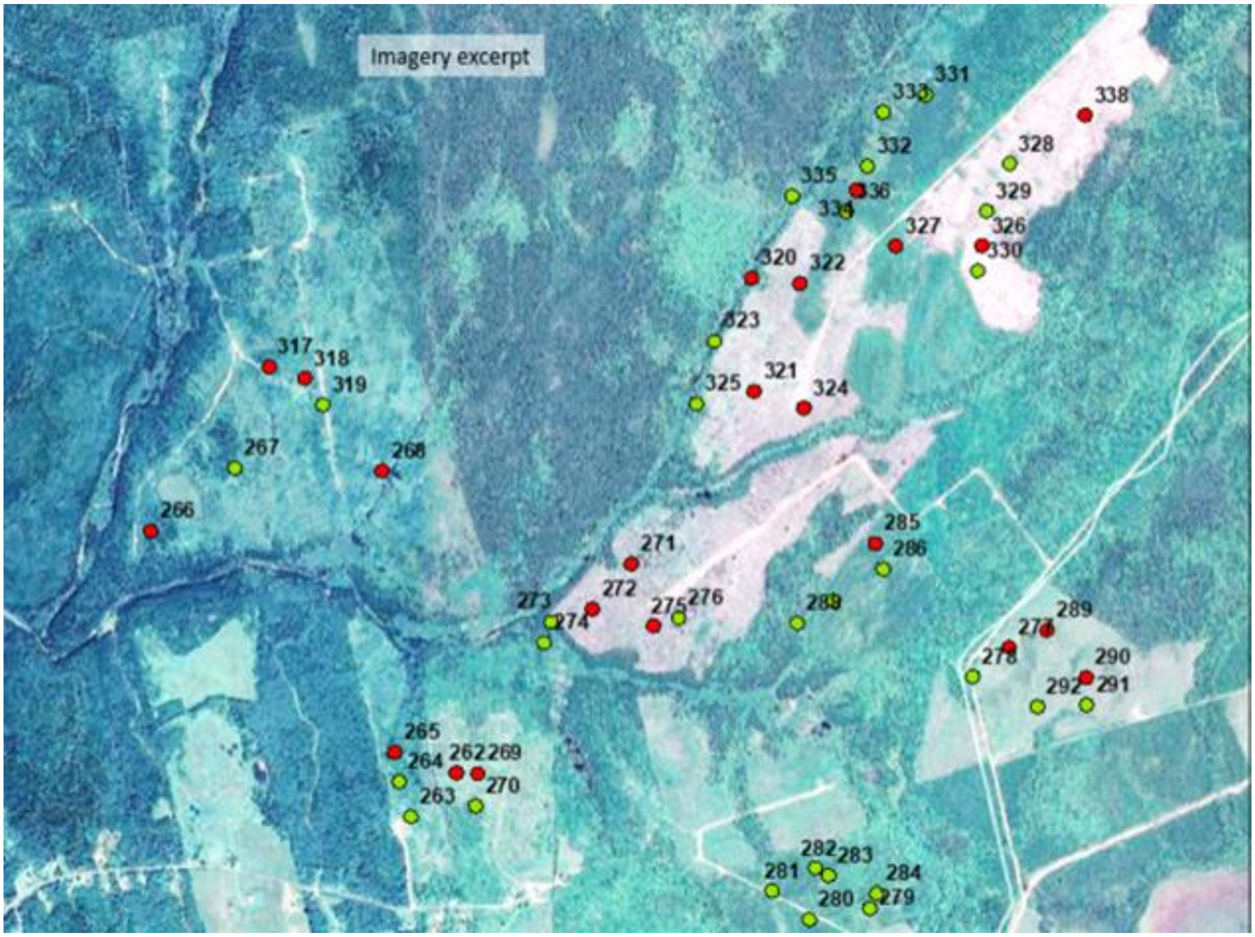

Figure 2. Example of imagery taken from the study area, showing points indicated as rutting (red) as well as the non-rutting points (green). Points in image also contain their FIDS.

Figure 2 illustrates in part the scope of the analysis, as cut blocks at varying stages of regeneration were investigated during the aerial imagery analysis. These varying cut blocks thus further required a standardized methodology in order to rank all instances of single pass rutting on an equal basis.

Figure 3. Further examples of the rutting and non-rutting points (indicated in red and green respectively). Image taken from the study area and points-enhanced in Microsoft word for illustrative purposes.

Binary logistic analysis was utilized as this analysis was focused solely on determining where rutting would occur with high probability. Simplifying the instances of rutting to yes/no or 1/0 delineation removes the speculation involved in determining the many variables that affect areas that may experience rutting.

Terrain Analysis

A polygon shapefile was used to extract the 1 m resolution elevation data from GeoNB's LiDAR DEM coverage for New Brunswick. The extracted layer was subsequently used to produce the depression, slope, flow direction, flow accumulation, flow channel, DTW, TPI, and TWI data layers using the appropriate ArcMap functions, as follows:

1. Depressions (Sinks) = DEM - filled DEM using ArcMap's Fill and Raster Calculator functions.
2. Flow direction (FD), based on 8 cardinal directions D8 Flow Direction function (Tarboron, 1997).
3. Flow accumulation (FA) using the Flow Accumulation function (Tarboron, 1997).
3. Flow channels, determined by re-classifying FA< =4 ha as no data, and FA> 4 ha as 1, followed by using the Raster to Polyline function.
4. Slope (in percent) using the Slope function.
5. DTW, using the Cost distance function with Slope as cost raster, and the > 4 ha flow channels as DTW = 0 reference (Murphy et al., 2009).
7. TWI = ln (FA/Slope), using the Raster Calculator function (Zimmerman and Shallenberger, 2016).
8. TPI = DEM – Mean 49 – 50 m Annulus Elevation around each DEM cell using the Focal Statistics and Raster Calculator functions (Weiss, 2001).
9. The GeoNB available forest soil data layer was converted from its shapefile into an NB-wide raster file, using the Feature to Raster conversion function.
10. The produced raster layers formed the based to tally the for slope, TWI, DTW, TPI and soil type conditions at each rut and no-rut location within the shapefile by way of the Extract Multipoint function.

To ensure further confidence in the predictive regression model, all points were visually inspected and if necessary, moved to be directly on top of any instances of rutting. In cases where the non-rutting points were located too closely to rutting points, theses points were also relocated to a more appropriate location further from any instances of rutting. Additionally, the LiDAR data used in this analysis, which is made available by the GeoNB database, was captured in 2015 meaning that deep ruts had the potential to be included in the DEM and the TPI. Thus, cut blocks with deep rutting occurrences dated before 2015 were excluded from the analysis.

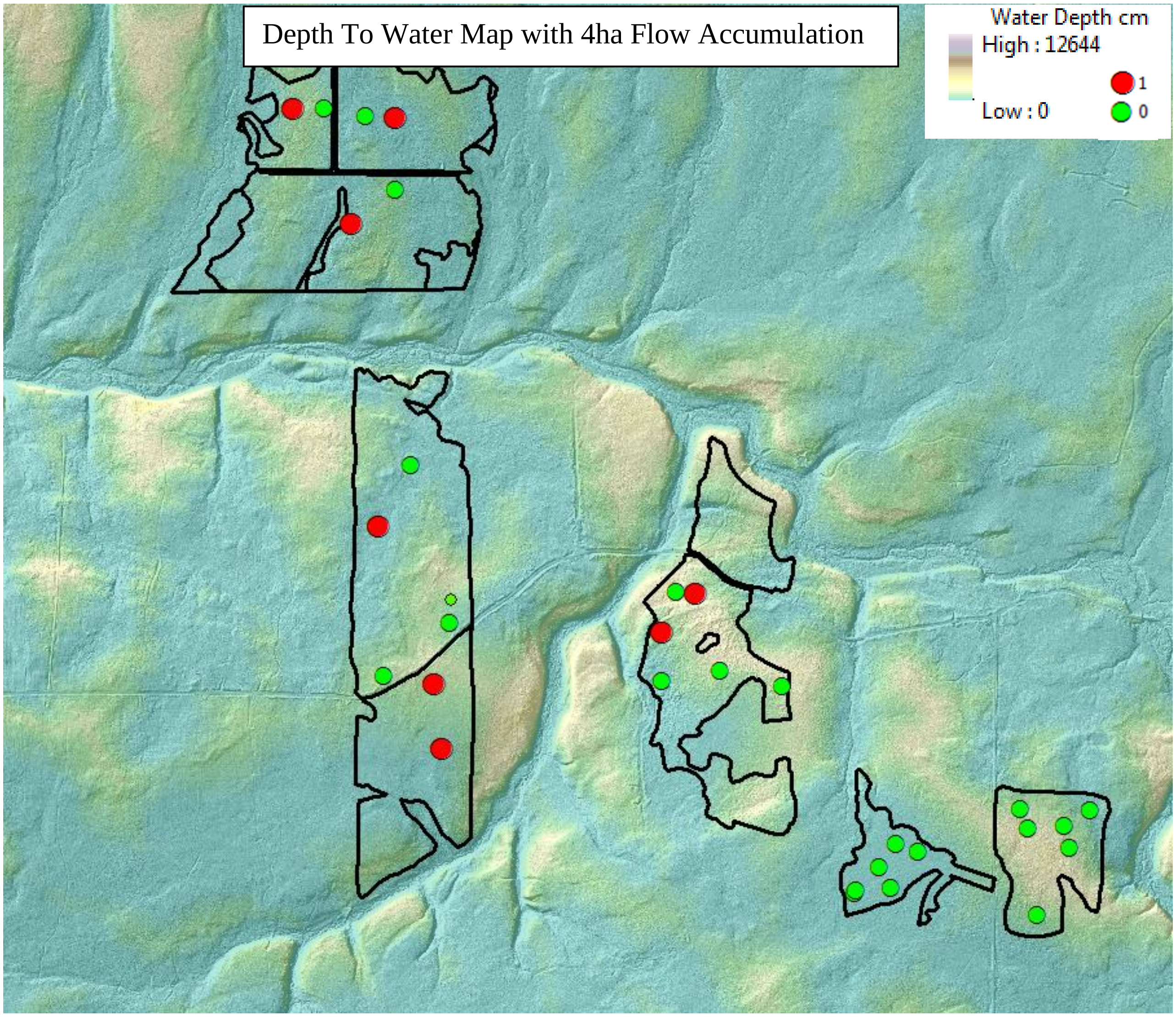

Figure 4. The cartographic depth to water map formulated using 4ha of upslope flow accumulation with the inclusion of several cut blocks (black outlines) as well as rutting points.

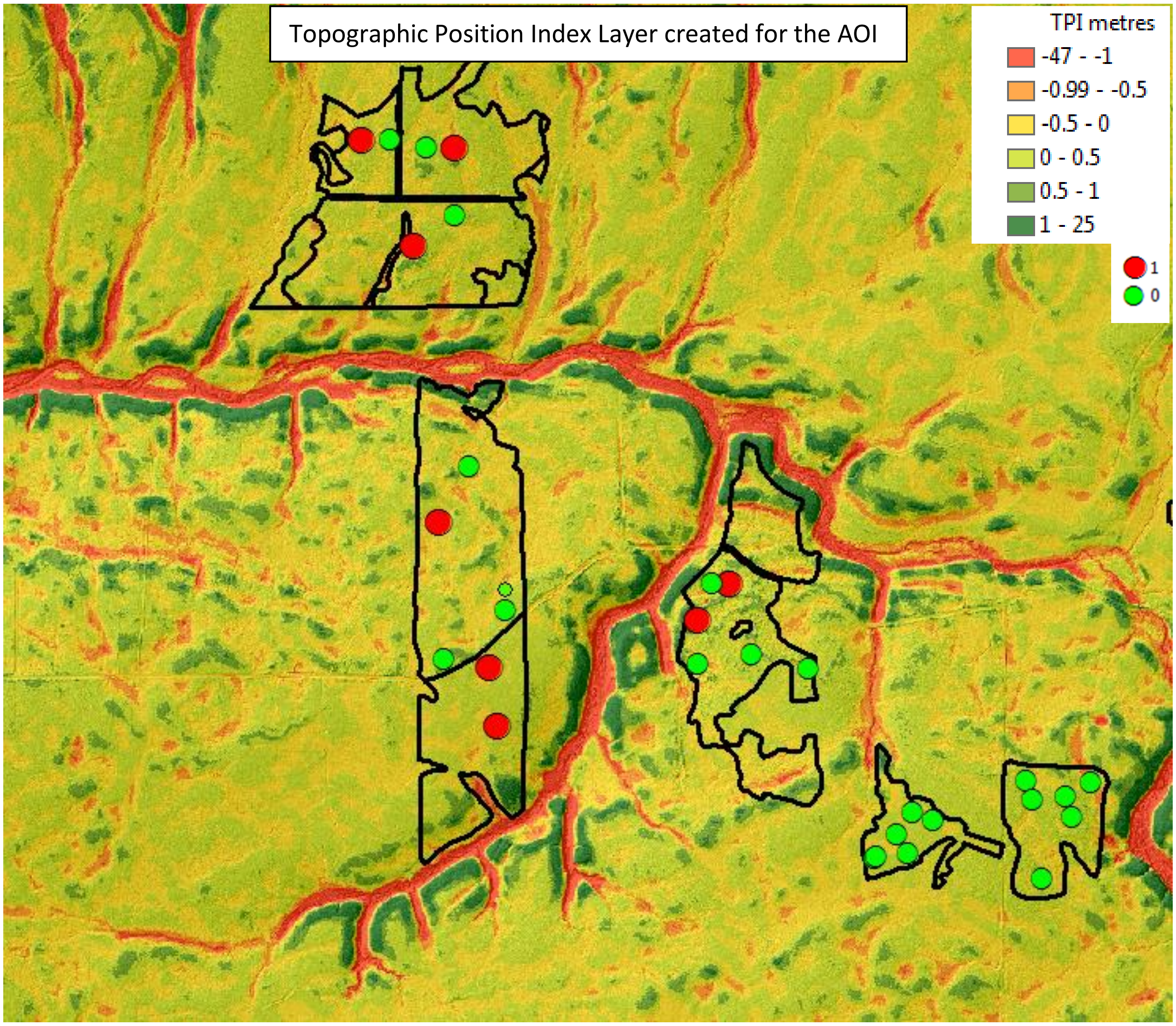

Figure 5. The topographic position index as created for the study area, with rutting points as well as cut blocks (black outline).

Statistical analysis

The rut, no-rut shapefile was saved as a text file, which was subsequently analyzed in Staview using the logistic regression analysis function, and using the following formulation:

y = ln[p/(1-p) = a + b sink + c slope + d (DTW4ha) + e TPI + f soil type + g TWI+ …

where

p = 1/(1+exb(-y) is the probability of rut occurrences.

Results

The best-fitted logistic regression results generated from Eq. 1 are displayed in Table 1. According to this, the likelihood of rutting can be inferred from two best-fitting predictor variables, namely the DEM-derived TPI and DTW formulations, with 84.93% reliability overall. The variables pertaining to soil type, slope and TWI when added to the analysis did not significantly change this result. In comparison, using the TPI variable as the only rut occurrence predictor was more discerning than using the DTW variable alone (Table 2 and Table 3). The overall correctness in classification dropped from 84.93% (TPI and DTW combined) to 81.65% (TPI only) and 69.17% (DTW only).

Table 1. Logistic regression result summary, with regression coefficient details about the best-fitting predictor variables and overall prediction classification for DTW and TPI combined.

Overall summary

Count	2926
# Missing	4
# Response Levels	2
# Fit Parameters	3
Log Likelihood	-1180.299
Intercept Log Likelihood	-1993.097
R Squared	0.408

Regression coefficients for the best-fitted variables

-	Coefficient	Std. Error	Coef/SE	Chi-Square	P-Value	Exp (Coef)
Constant	0.156	0.081	1.926	3.711	0.0540	1.168
TPI	-4.533	0.187	-24.266	588.835	<0.0001	0.01
DTW(4ha)	-0.003	2.516E-4	-13.225	174.911	<0.0001	0.997

Best-fitted prediction classification

-	Predicted 0	Predicted 1	Percent Correct
Observed 0	1484	205 (false negatives)	87.86%
Observed 1	236 (false positives)	1001	80.92%
Overall	-	-	84.93%

Best-fitted logistic regression equation:

$$y = 0.156 - 4.53\ \text{TPI (in m)} - 0.33\ \text{DTW (in m)};\ R^2 = 0.41 \qquad [1]$$

Table 2. Logistic regression result summary, with regression coefficient details about TPI as only best-fitting predictor variable and overall prediction classification.

Overall summary

Count	2926
# Missing	4
#Response Levels	2
# Fit Parameters	2
Log Likelihood	-1286.469
Intercept Log Likelihood	-1993.097
R Squared	0.355

Regression coefficients for TPI as only best-fitted variable

-	Coefficient	Std. Error	Coef/SE	Chi-Square	P-Value	Exp (Coef)
Constant	-0.707	0.052	-13.543	183.403	<0.0001	0.493
TPI	-4.635	0.183	-25.270	638.554	<0.0001	0.010

Best-fitted prediction classification with TPI as only rut occurrence predictor

-	Predicted 0	Predicted 1	Percent Correct
Observed 0	1466	223 (false negatives)	86.80%
Observed 1	314 (false positives)	923	74.62%
Overall	-	-	81.65%

Best-fitted logistic regression equation:

$$y = 0.707 - 4.63 \text{ TPI (in m)}; R^2 = 0.355 \qquad [2]$$

Table 3. Logistic regression result summary, with regression coefficient details about DTW as only best-fitting predictor variable and overall prediction classification.

Overall summary

Count	2926
# Missing	4
#Response Levels	2
# Fit Parameters	2
Log Likelihood	-1794.557
Intercept Log Likelihood	-1993.097
R Squared	0.100

Regression coefficients for DTW as only best-fitted variable

-	Coefficient	Std. Error	Coef/SE	Chi-Square	P-Value	Exp (Coef)
Constant	0.672	0.066	10.169	103.413	<0.0001	1.957
DTW 4ha	-0.004	2.117E-4	-16.778	281.506	<0.0001	0.996

Best-fitted prediction classification with DTW as only rut occurrence predictor

-	Predicted 0	Predicted 1	Percent Correct
Observed 0	1301	388 (false negatives)	77.03%
Observed 1	514 (false positives)	723	58.45%
Overall	-	-	69.17%

Best-fitted logistic regression equation:

$$y = 0.672 - 4.63 \text{ DTW (in m)}; R^2 = 0.355 \qquad [3]$$

Averaging the point-by-point rut probability results in 0-5%, 5-10%, 10-15% classes and averaging the 0,1 rut occurrences accordingly produced the rut and no rut plots in Figure 6. This plot confirms, visually, how the Eq.1 modelled rut occurrence probability conforms in extent to the image-ascertained rut locations overall. Examples of how the individual rut versus no-rut point observations compare with the mapped expression of Eq. 1 are shown in Figures 6-11.

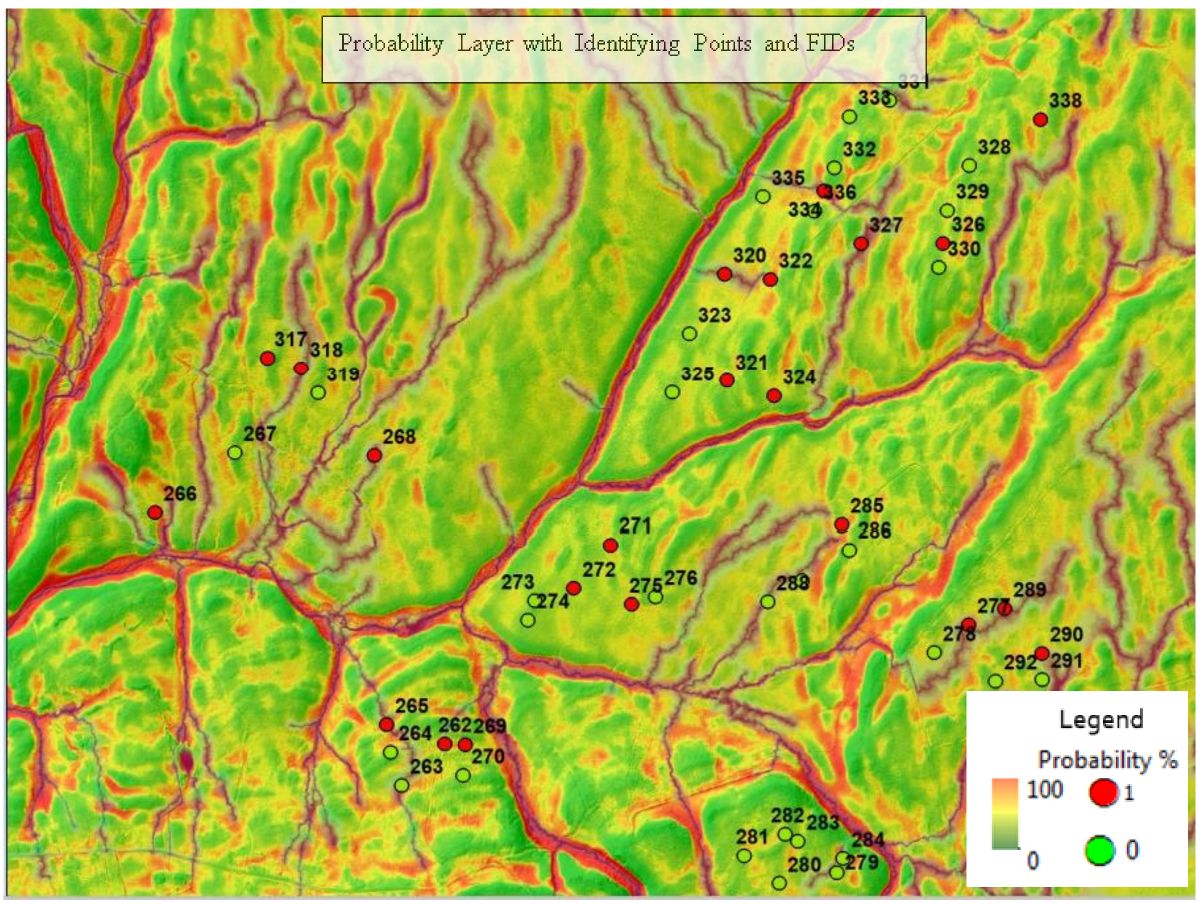

Figure 6. The created rutting probability raster layer, overlain on the hill-shade LiDAR DEM, areas deemed to have a high probability of rutting are red, and low probability of rutting is

indicated in green. Red points are observed rutting locations and green points are observed non-rutting sites

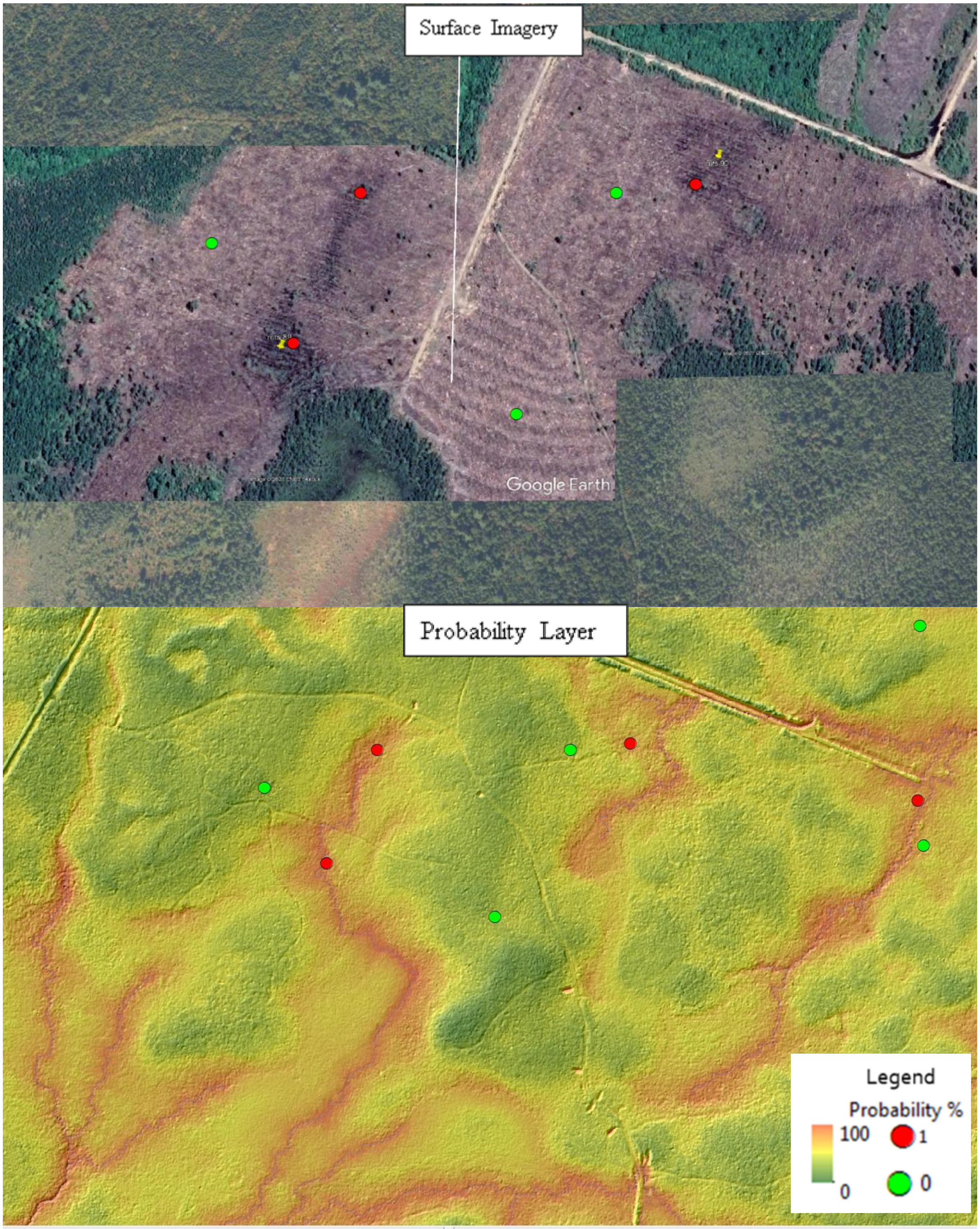

Figure 7. Surface image of an affected cut block (top), with rutting locations are indicated in red points and non-rutting is indicated by green points (Bottom). The same cut block with the logistic regression model formulated probability layer overlain on the hill shade relief layer. Rutting

probability varies from 0% in the green sections to 100% in the red sections. (Yellow pushpins indicate additional rut markings and are residual from the Google Earth analysis).

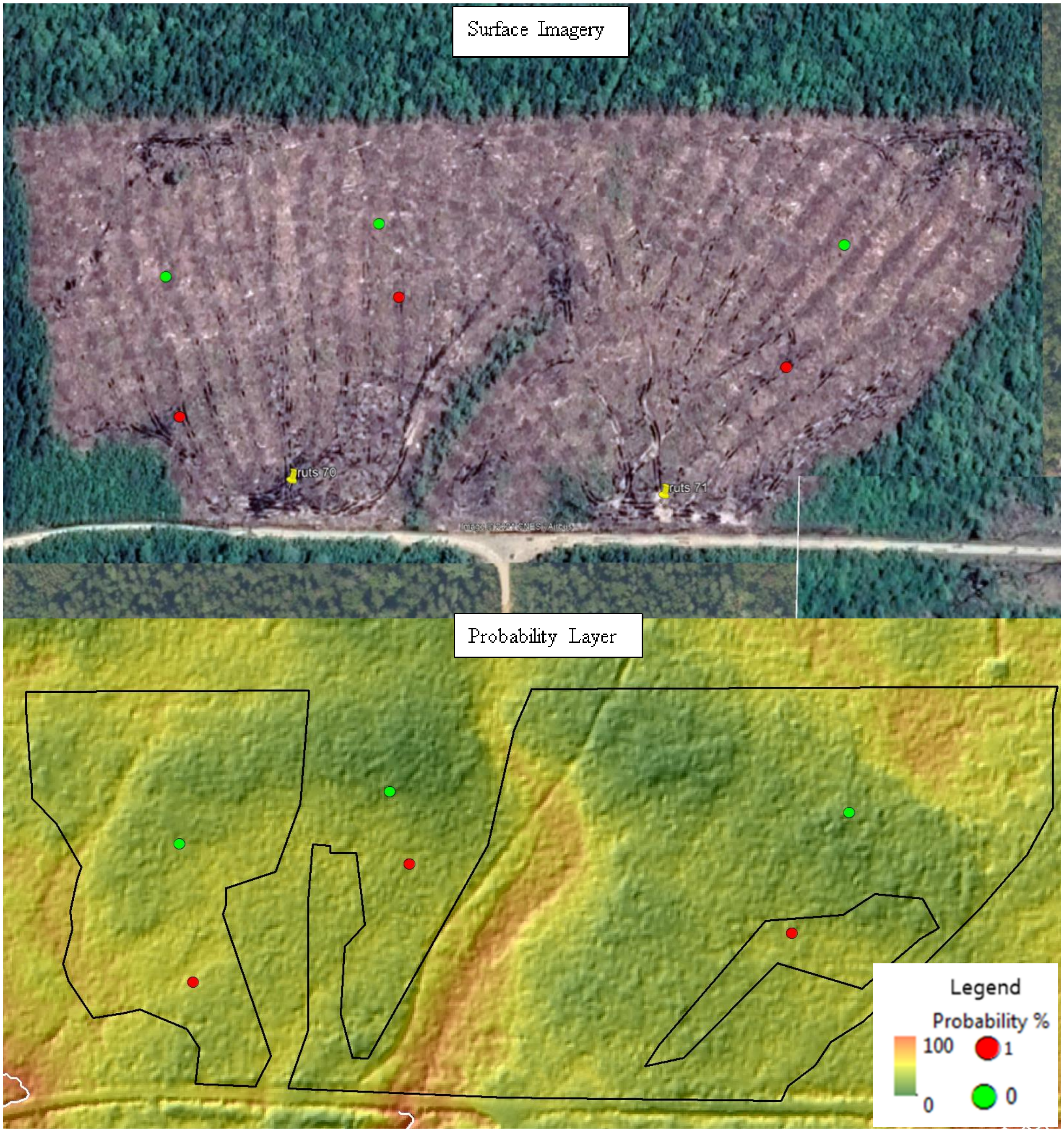

Figure 8. Surface image (top) compared to probability layer (below), with selection of markers indicating ruts (red) and no ruts (green).

Figures 7 and 8 illustrate the abilities of this probability model to determine low-laying areas as well as significantly wetted areas, which have been identified as conditions conducive to the formation of soil rutting and are consistent with the wetted and rutting areas located through the surface imagery.

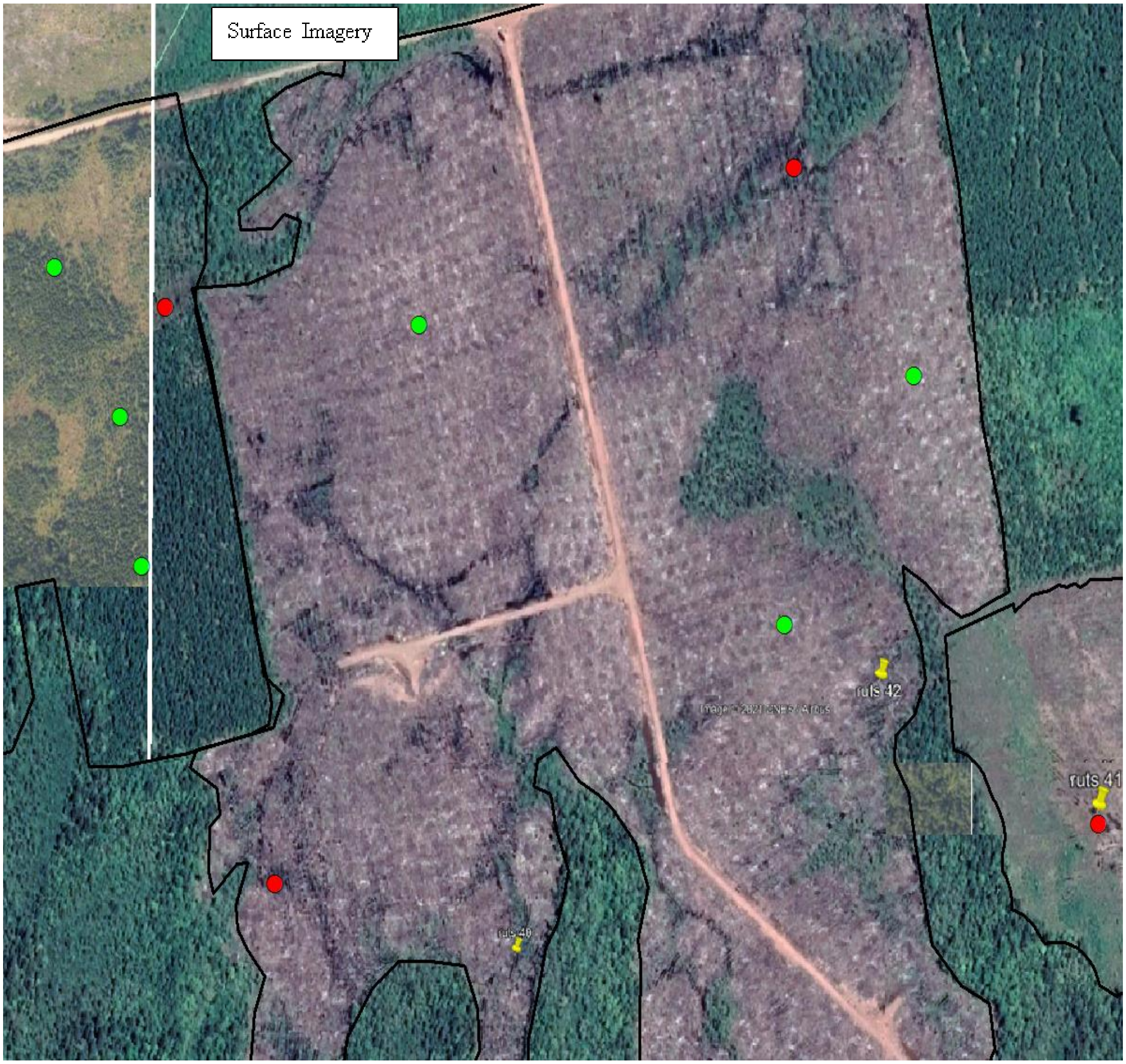

Figure 9a. Surface image showing extent of soil rutting, with selection of markers indicating ruts (red) and no ruts (green)

Items of note in Figure 9a are the flow channels that indicate wetted areas as well as the logging access road that is centrally located within the cut block. The flow networks and other significantly wetted areas appear in Figure 9b, as to demonstrate the effectiveness of this model in locating these areas of significant flow accumulation and lower microtopography. These conditions are seen to coincide with the instances of rutting captured in the aerial imagery for this example.

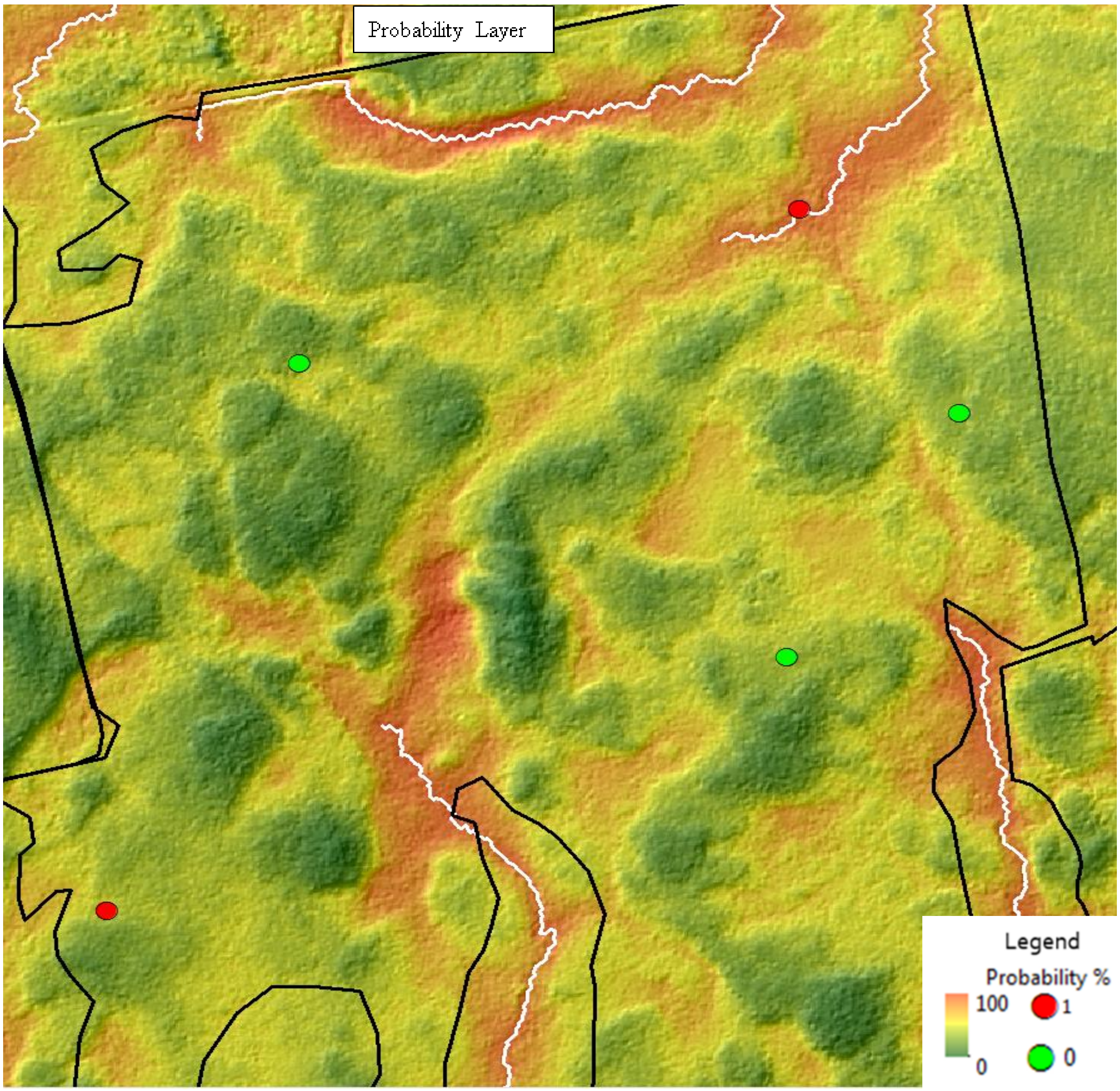

Figure 9b. Rut probability layer, with selection of markers indicating ruts (red) and no ruts (green).

The flow networks and low-laying areas in Figure 9a were noted to experience rutting as delineated in the rut occurrence probability layer. The lack of DEM-apparent roads in Figure 9b indicates that this area was harvested after the LiDAR data was acquired in 2015. Thus, the rut occurrence probability model is able to effectively predict areas with high probability of rutting before the start-up cut block access and harvesting operations.

Figures 10 and 11 demonstrate the same effectiveness in the probability mapping as Figures 9a and b, however the LiDAR data in Figure 10 was taken after the area had been harvested as indicated by the presence of the created logging road towards the bottom of the image. This road was not likely to cause any significant effect on the LiDAR data concerning rutting probability as this road did not intersect the cut block. However, similar to Figure 9, Figure 11 does not have the logging road present in its LiDAR data and thus, the model was able to effectively predict areas of rutting under pre-harvesting conditions using the DTW and TPI derived probability layer. Reviewing the results listed in Tables 1, 2 to 3 indicates the TPI more effective than DTW in correctly classifying rut occurrences, i.e., leading 81.7% and 69.2% correct classifications, respectively. This being so, combining TPI with DTW as logistic regression predictor variables further enhances the overall rut occurrence classification to 84.9%.

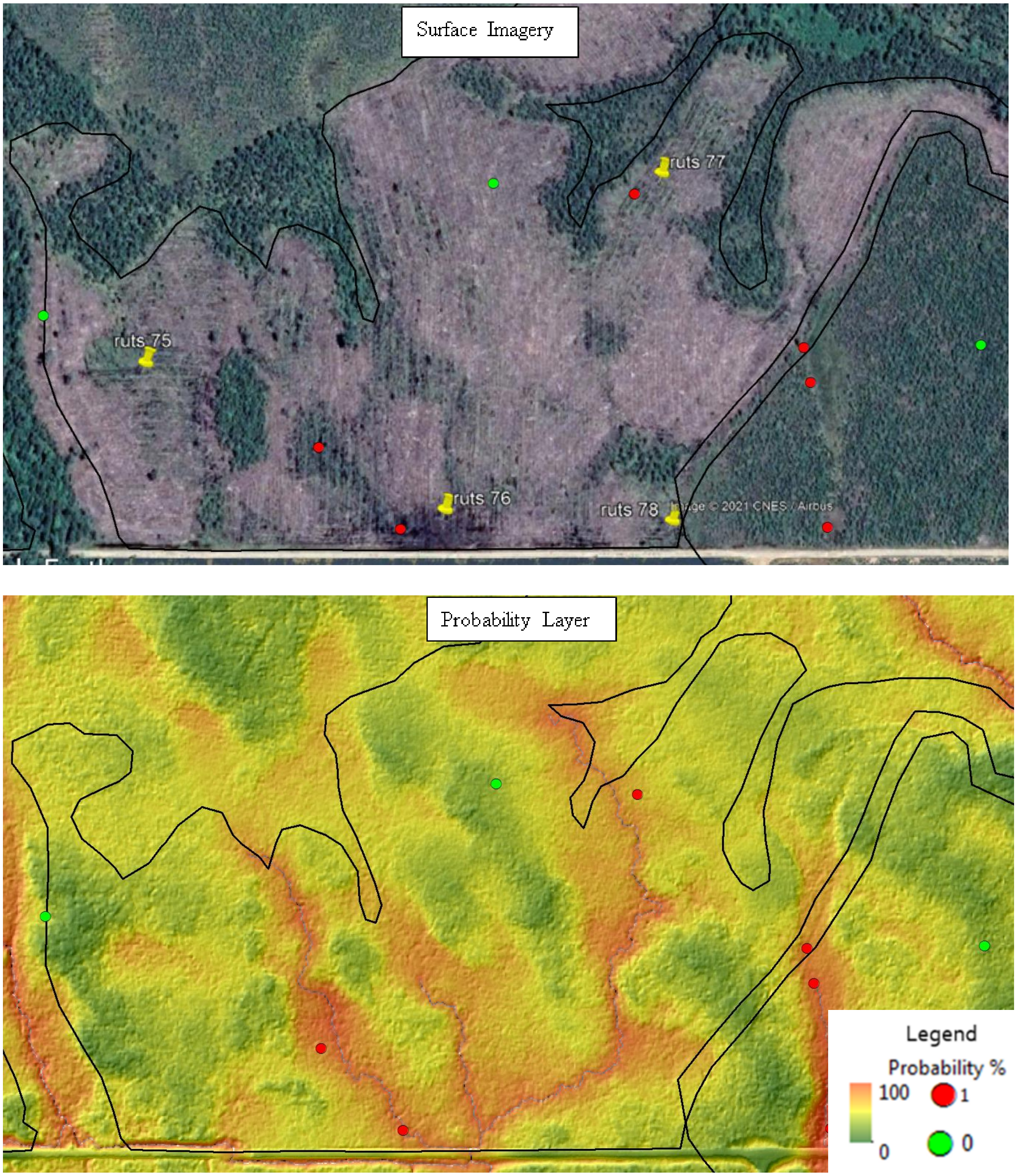

Figure 10. Surface image compared to probability layer, and selection of markers indicating ruts (red) and no ruts (green).

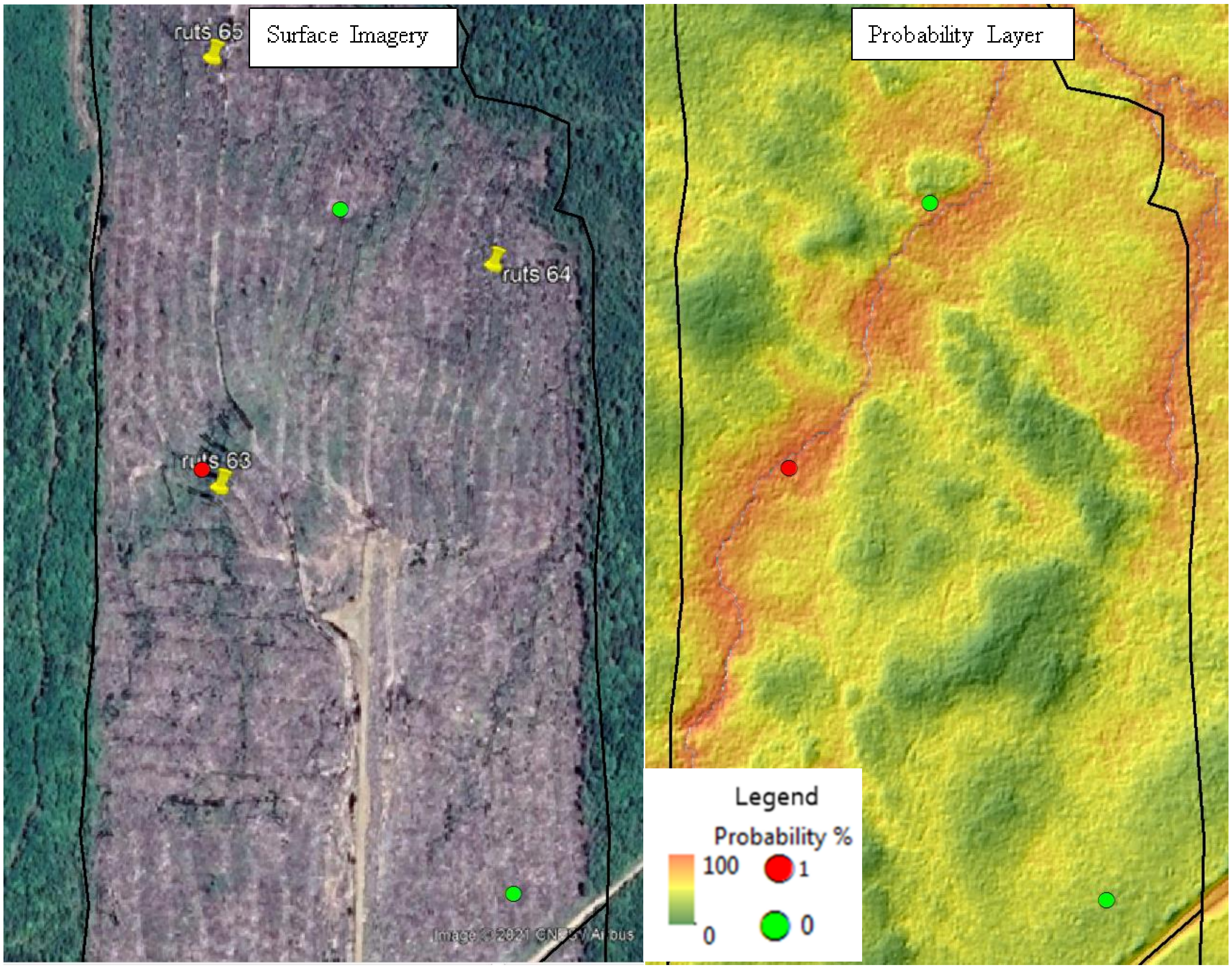

Figure 11. Surface image compared to probability layer with selection of markers indicating ruts (red) and no ruts (green).

Discussion

As evidenced by Figures 6 - 11, the regression derived probability map conforms to the aerial imagery of rutting fields and is thus generally effective in predicting soil rutting based on the local variations in microtopography. Testing soil type as additional logistic regression predictor variable for rut occurrences did not affect the results summarized in Tables 1 to 3 significantly. This could be due to the location of the study area, which is mainly comprised of the New Brunswick eastern lowlands: a floodplain with low-laying topography generally underlain by compacted till (basal till;

Figure 12). Thus, while soil type may have a greater effect on the soil moisture content in areas with highly variable topography, it does not appear to have the same effect on this region. As such, lowland depressions as revealed by TPI mapping across the survey area tend to accumulate and retain water for longer periods of to time than depressions across well drained areas. Since many of these depressions exist between the > 4 ha defining upslope flow-accumulation area criterion for permanent streams, it is clear how TPI mapping for rut occurrences would complement the DTW < 1 m delimited wet-area extent along permanent streams.

Overall, the TPI and DTW 4ha delineations both inform about low-lying areas in which water accumulates and remains. In contrast, the 0.25 ha and 1ha upslope flow accumulation DTW maps do not significantly affect the logistically determined soil rutting potential as the water that would accumulate in the additional areas so mapped would, for the most part, not remain for extended periods of time.

Figure 12 illustrates the position of the study area within the greater topographical context of New Brunswick. The majority of the study resides in this area of lower topography which may be a factor as to why the slope, and subsequently the TWI, were not deemed as significant variables in this analysis. Lower variation in topography could have amplified the propensity for water to accumulate in the low points of micro-topography given the minimal slope of the study area which can be seen in Figure 13.

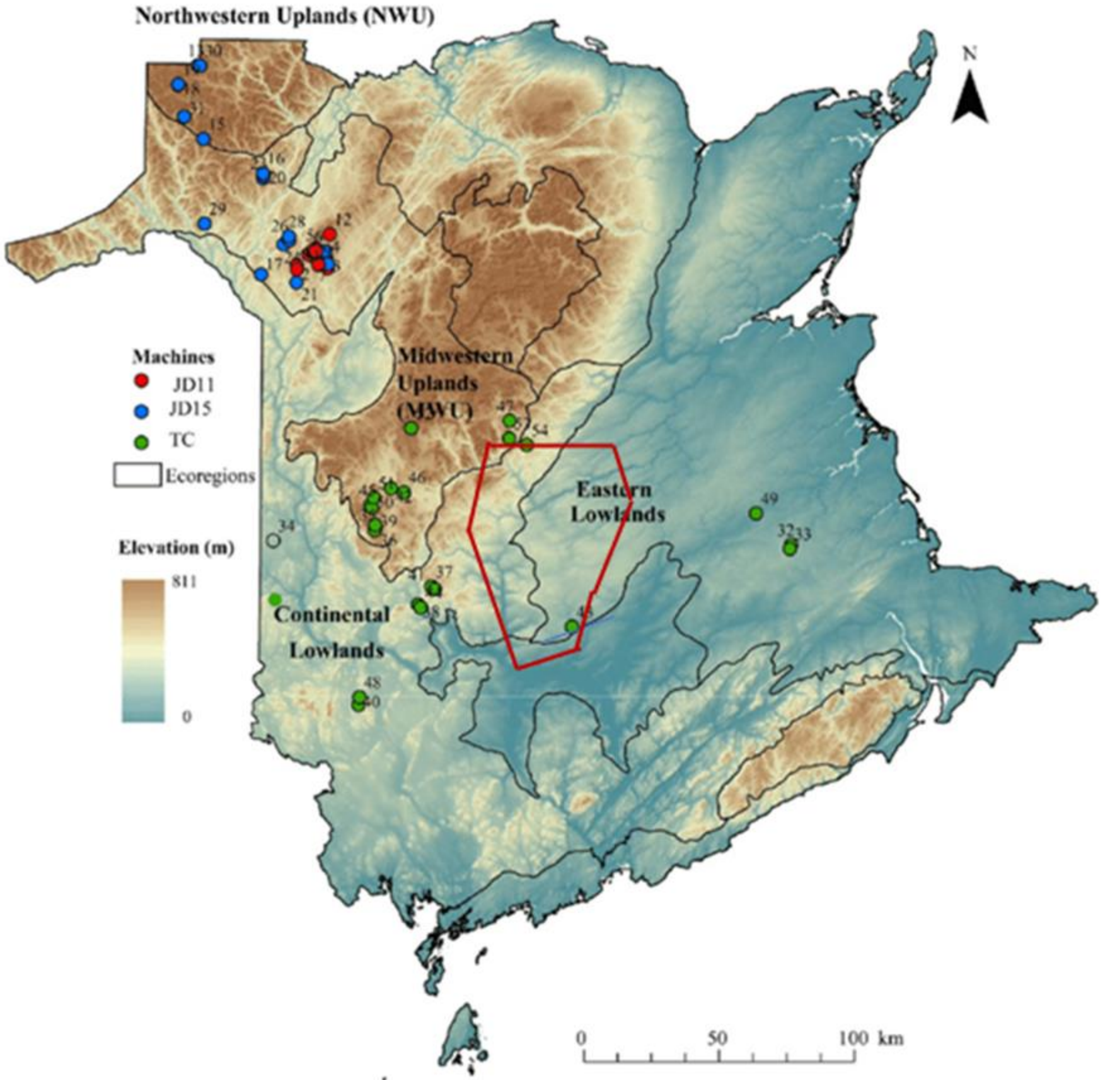

Figure 12. Topographic map of New Brunswick indicating the eastern lowlands ecoregion with study area (red polygon) overlain. (Jones, 2018).

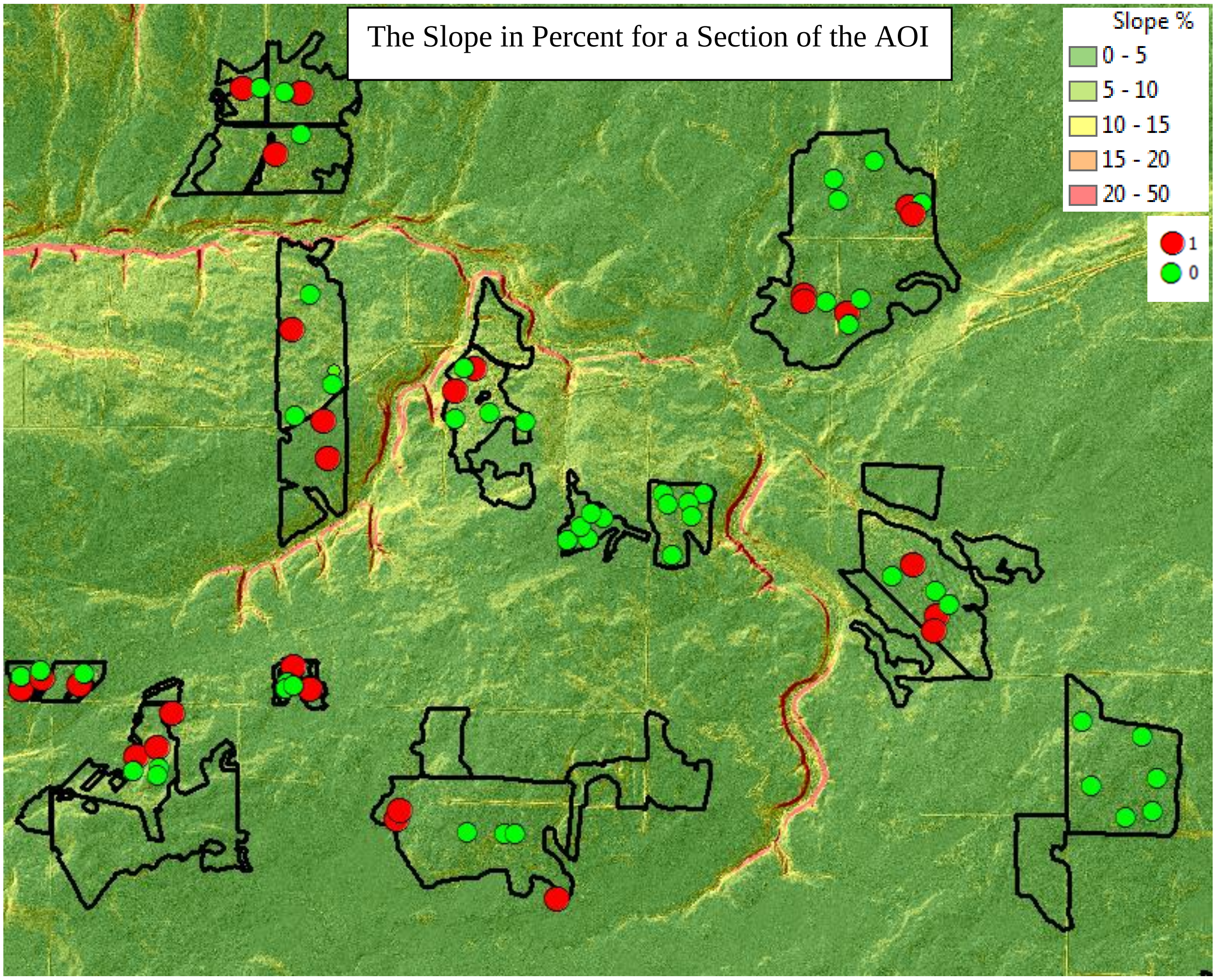

Figure 13. The slope for an area of the analysis, showing cut blocks (black outline) as well as several rutting points. This figure shows the pattern of relatively minimal slope within the AOI.

The classification of false positives and negatives in Table 1 attests to DEM-triggered TPI and DTW interpretation limitations:

1. TPI classified high "rut" occurrence probabilities at steep foot slope locations are likely false positive artifacts because the negative TPI values at these locations are due to averaging across the steep and flat portions along these locations.
2. The TPI index loses its depression- and ridge-locating power across flat areas wider than the 100 m TPI-determining annulus diameter: here, TPI values tend to be at or near 0 m

(generally mapped yellow in Figures 6 to 11). Hence, small elevated and depressed area would not be TPI- recognized in terms of potential rut occurrences, thus leading to false negatives at actual rut locations, and false positives at no rut locations.

3. DEM-indicated flow blockages such as roads or beaver dams can divert permanent streamflow channels from their true paths, thus
   (i) marking the areas next to the resulting DEM-traced flow channels to be wet, therefore leading to false positives, and
   (ii) the areas next to the actual but DEM non-traced flow channels dry, therefore leading to false negatives.

Future Applications

While the TPI and DTW 4ha layers were successful in determining the probability of rutting 85% of the time, further additions to the model could yield in a useful predictive tool for scheduling harvesting operations. In all of this, it should be remembered that in areas where Eq.1 predicted high probabilities of rutting, making ruts can essentially be avoided when soil and weather conditions at the time of operations are favorable. Favorable conditions refer to when the soils are frozen, and when the soils are sufficiently dry. The inclusion of weather data in conjunction with the current predictive model would produce a dynamic trafficability map (Labelle et al., 2022). Currently, there are available hydrological and meteorological data that could be used in conjunction with the probability layer to determine where rutting may form based on current, local conditions. For example, the inclusion of local weather data in a trafficability map would be beneficial as changes in daily, weekly, monthly, and seasonal precipitation and temperatures affect the extent of soil compaction (Hansson et al., 2018, Allman et al., 2017, Toivio et al., 2017, Hansson et al., 2018, Marchi et al., 2018, Jankovský et al., 2019, Ilintsev et al., 2020, Labelle et al., 2022). Furthermore, increased variability in weather patterns brought on by anticipated climatic changes can further affect soil moisture and may shorten the window for harvesting operations (Marchi et al., 2018, Ilintsev et al., 2020, Toivio et al., 2017 as cited in Labelle et al., 2022). An additional use for this type of mapping would be to delineate habitats by fauna and flora specific moisture regime preferences, thus lending this tool to interdisciplinary applications.

Conclusion

The logistic regression analysis of rut occurrences in cut blocks across the area of interest in this study, using LiDAR-derived TPI and cartographic DTW layers, have shown to be effective in capturing the incidences of rutting 85% of the time. The TPI layer identifies areas with lower microtopography where soil water has a higher chance of aggregating and the DTW 4ha layer identifies these permanently wetted areas near rivers, streams, lakes, and wetlands. In this analysis, the DEM-derived TPI and DTW data layers were the only significant rut occurrence predictors. Adding soil type, slope and TWI to this analysis did not significantly improve on predicting where ruts and no ruts actually occurred. This can potentially be explained by the glacial till mode of deposition combined with the overall lower topography of the study area.

False positives and negatives can be attributed to variations and anomalies in local microtopography as well as temporal variations in soil moisture content due to weather conditions. Since the resulting map quantifies where rutting is likely to occur across the study area, it may become an important tool in terms of planning how to minimize / eliminate rut occurrences along trails and roads within and towards cut blocks. Thus, a dynamic model that includes site specific conditions pertaining to hydrology and weather data will become a useful tool for scheduling operations, especially with the closing window for wintertime harvests forecasted with climate change. Further studies are needed to determine the extent to which the rut occurrence model based on Eq. 1 applies to observing cut block ruts in other areas, whether located in New Brunswick or elsewhere.

References

Allman, M., Jankovský, M., Messingerová, V., Allmanová, Z. (2017). Soil moisture content as a predictor of soil disturbance caused by wheeled forest harvesting machines on soils of the Western Car- pathians. *Journal of Forestry Research*. 28:283–9. Doi: 10.1007/s11676-016-0326-y

Ares, A., Terry, T.A., Miller, R.E., Anderson, H.W. & Flaming, B.L. (2005). Ground-based Forest harvesting effects on soil physical properties and Douglas- fir growth. *Soil Science Society of America Journal* 69: 1822–1832. doi:10.2136/sssaj2004.0331

Batey, T. (2009) Soil compaction and soil management: a review. *Soil Use Management.* 25:335–345. https://doi.org/10.1111/j.1475-2743.2009.00236.x

Beven, K., Kirkby, M.J., (1979). A physically based, variable contributing area model of basin hydrology. *Hydrological Sciences Journal*. 24 (1), 43–69. doi:10.1080/02626667909491834

Bottinelli, N., Hallaire, V., Goutal, N., et al. (2014). Impact of heavy traffic on soil macroporosity of two silty forest soils: initial effect and short-term recovery. *Geoderma* 217–218:10–17. https://doi.org/10.1016/j.geoderma.2013.10.025

Cambi, M., Giannetti, F., Bottalico, F., et al, (2018a) Estimating machine impact on strip roads via close-range photogrammetry and soil parameters: a case study in central Italy. *Iforest* 11:148–154. https://doi.org/10.3832/ifor2590-010

Cambi, M., Mariotti, B., Fabiano, F., et al. (2018b). Early response of Quercus robur seedlings to soil compaction following germination. *Land Degradation and Development*. doi:10.1002/ldr.2912

Campbell, D. M. H., White, B., & Arp, P. A. (2013). Modeling and mapping Soil resistance to penetration and rutting using LiDAR-derived digital elevation data. *Journal of Soil and Water Conservation*, *68*(6), 460–473. https://doi.org/10.2489/jswc.68.6.460

Duncker, P.S., Raulund-Rasmussen, K., Gundersen, P., Katzensteiner, K., De Jong, J., Ravn, H.P., et al. (2012). How forest management affects ecosystem services, including timber production and economic return: synergies and trade-offs. *Ecology and Society*. 17(4), 50. doi: 10.5751/ES-05066-170450

Ezzati, S., Najafi, A., Rab, M. A., & Zenner, E. K. (2012). Recovery of soil bulk density, porosity and rutting from ground skidding over a 20-year period after timber harvesting in Iran. *Silva Fennica*, *46*(4), 521–538. https://doi.org/10.14214/sf.908

Goutal, N., Keller, T., Défossez, P. and Ranger, J. (2013). Soil compaction due to heavy forest traffic: measurements and simulations using an analytical soil compaction model. *Annals of. Forest Science*. 70(5), 545–556. doi: 10.1007/s13595-013-0276-x.

Government of Canada: Environment. and Natural Resources. (2021). Canadian Climate Normals 1981-2010 Station Data. Retrieved from climate.weather.gc.ca: https://climate.weather.gc.ca/climate_normals/results_1981_2010_e.html?searchType=stn

Prov&lstProvince=NB&txtCentralLatMin=0&txtCentralLatSec=0&txtCentralLongMin=0&txtCentralLongSec=0&stnID=6106&dispBack=0

Hansson, LJ., Ring, E., Franko, MA., Gärdenäs, AI. (2018). Soil temperature and water content dynamics after disc trenching a sub-xeric Scots pine clearcut in central Sweden. *Geoderma*. 327:85–96

Ilintsev, A., Bogdanov, A., Nakvasina, E., Amosova, I., Koptev, S., Tretyakov, S. (2020). The natural recovery of disturbed soil, plant cover and trees after clear-cutting in the boreal forests. *Russia iForest*. 13:531–40

Jankovský, M., Allman, M., Allmanová, Z., Ferenčík, M., Vlčková, M. (2019). Changes of key soil parameters five years after forest harvest- ing suggest slow regeneration of disturbed soil. *Journal of Sustainable Forestry*. 38:369–80.

Jansson, KJ., Wasterlund, I. (1999). Effect of traffic by lightweigth foret machinery on the growth of young Picea abies trees. *Scandanavian Journal of Forest Research.* 14:581–588

Jones, M-F., & Castonguay, M., Jaeger, D., Arp, P. (2018). Track-Monitoring and Analyzing Machine Clearances during Wood Forwarding. *Open Journal of Forestry*. 08. 297-327. 10.4236/ojf.2018.83020.

Jourgholami, M., Khajavi, S., Labelle, ER. (2020). Recovery of forest soil chemical properties following soil rehabilitation treatments: an assessment six years after machine impact. *Croatian Journal of Forest Engineering.* 41:163–175.

Kauppinen, J., Väätäinen, K., Tauriainen, S., Einola, K., Malinen, J. and Sirén, M. (2016). Importance of multi-source information and map-based operator assistance in mechanised wood harvesting [in finnish] Monilähdetietoa hyödyntävien karttaopasteiden tarve puunkorjuussa. Luonnonvara- ja biotalouden tutkimus 15/2016, *Luonnonvarakeskus*. Abstract in English available at: http://urn.fi/URN:ISBN: 978–952–326-196-9

Labelle, E.R. and Jaeger, D. (2011). Soil compaction caused by cut-to- length forest operations and possible short-term natural rehabilitation of soil density. *Soil Science Society of America Journal*. 75(6), 2314–2329. doi: 10.2136/ss- saj2011.0109

Labelle, E. R., Hansson, L., Högbom, L., Jourgholami, M., & Laschi, A. (2022). Strategies to Mitigate the Effects of Soil Physical Disturbances Caused by Forest Machinery: a Comprehensive Review. *Current Forestry Reports*. *8*(1), 20–37. https://doi.org/10.1007/S40725-021-00155-6

Launiainen, S., Guan, M., Salmivaara, A. and Kieloaho, A.-J. (2019). Modeling forest evapotranspiration and water balance at stand and catchment scales: a spatial approach. *Hydrology and Earth Systems Science*. 23(8), 3457–3480. doi: 10.5194/hess-23-3457-2019

Lee, E., Li, Q,, Eu, S., et al. (2020). Assessing the impacts of log extraction by typical small shovel logging system on soil physical and hydro- logical properties in the Republic of Korea. *Heliyon.* 6:e03544. https:// doi. org/ 10. 1016/j. heliy on. 2020. e03544

Lehtonen, I., Venäläinen, A., Kämäräinen, M., Asikainen, A., Laitila, J., Anttila, P., & Peltola, H.

(2019). Projected decrease in wintertime bearing capacity on different forest and soil types in Finland under a warming climate. *Hydrology and Earth System Sciences*, *23*(3), 1611–1631. https://doi.org/10.5194/hess-23-1611-2019

Marchi, E., Chung, W., Visser, R., et al, (2018). Sustainable forest operations (SFO): a new paradigm in a changing world and climate. *Science of the Total Environment*. 634:1385–1397. https:// doi.org/10.1016/j.scito tenv.2018.04.084

Marion, J.L., and N. Olive. (2006). Assessing and understanding trail degradation: Results from Big South Fork National River and Recreational Area. Reston, VA: United States Department of the Interior. US Geological Survey. Patuxent Wildlife Research Center. Virginia Tech Field Unit. National Park Service. Final Research Report. http://www.parks.ca.gov/pages/1324/files/f10602%20 marion&olive.pdf

Mariotti, B., Hoshika, Y., Cambi, M., et al. (2020). Vehicle-induced compaction of forest soil affects plant morphological and physiological attributes:attributes: a meta-analysis. *Forest Ecolology Management.* 462:118004. https://doi.org/10.1016/j.foreco.2020.118004

Marra, E., Laschi, A., Fabiano, F., Foderi, C., Neri, F., Mastrolonardo, G., Nordfjell, T., & Marchi, E. (2021). Impacts of wood extraction on soil: assessing rutting and soil compaction caused by skidding and forwarding by means of traditional and innovative methods. *European Journal of Forest Research*. https://doi.org/10.1007/s10342-021-01420-w

Mattila, U., & Tokola, T. (2019). Terrain mobility estimation using TWI and airborne gamma-ray data. *Journal of Environmental Management*, *232*, 531–536. https://doi.org/10.1016/j.jenvman.2018.11.081

Morgan, R. P., Rasin, V. J., & Noe, L. A. (1983). Sediment Effects on Eggs and Larvae of Striped Bass and White Perch. *Transactions of the American Fisheries Society*, *112*(2A), 220–224. https://doi.org/10.1577/1548-8659(1983)112<220:seoeal>2.0.co;2

Murphy, P. N. C., Ogilvie, J., & Arp, P. (2009). Topographic modelling of soil moisture conditions: A comparison and verification of two models. *European Journal of Soil Science*, *60*(1), 94–109. https://doi.org/10.1111/j.1365-2389.2008.01094.x

Niemi, M. T., Vastaranta, M., Vauhkonen, J., Melkas, T., & Holopainen, M. (2017). Airborne LiDAR-derived elevation data in terrain trafficability mapping. *Scandinavian Journal of Forest Research*, *32*(8), 762–773. https://doi.org/10.1080/02827581.2017.1296181

Nugent, C., Kanali, C., Owende, P. M., Nieuwenhuis, M. and Ward, S. (2003). Characteristic site disturbance due to harvesting and extraction machinery traffic on sensitive forest sites with peat soils. *Forest Ecology and Management*. 180(1–3), 85–98. doi:10.1016/S0378-1127(02)00628-X.

Pundir, S. K., & Garg, R. D. (2021). Development of rule based approach for assessment of off-road trafficability using remote sensing and ancillary data. *Quaternary International*, *575–576*(June 2020), 308–316. https://doi.org/10.1016/j.quaint.2020.07.017

Riggert, R., Fleige, F., Kietz, B., Gaertig, T. and Horn, R. (2016). Stress distribution under forestry machinery and conse- quences for soil stability. *Soil Science Society of* America Journal. 80(1), 38–47. doi: 10.2136/sssaj2015.03.0126

Salmivaara, A., Launiainen, S., Perttunen, J., Nevalainen, P., Pohjankukka, J., Ala-Ilomäki, J., Sirén, M., Laurén, A., Tuominen, S., Uusitalo, J., Pahikkala, T., Heikkonen, J., & Finér, L. (2021). Towards dynamic forest trafficability prediction using open spatial data, hydrological modelling and sensor technology. *Forestry*, *93*(5), 662–674. https://doi.org/10.1093/FORESTRY/CPAA010

Sirén, M., Ala-Ilomäki, J., Mäkinen, H., Lamminen, S. and Mikkola, T. (2013). Harvesting damage caused by thinning of Norway spruce in unfrozen soil. *International Jounral of Forest* Engineering. 24(1), 60–75. doi: 10.1080/19132220.2013.792155

Solgi, A., Naghdi, R., Marchi, E., et al. (2019). Impact assessment of skid- ding extraction : effects on physical and chemical properties of forest soils and on maple seedling growing along the skid trail. *Forests* 10:1–17. https:// doi. org/ 10. 3390/ f1002 0134

Sugai, T., Yokoyama, S., Tamai, Y., et al. (2020) Evaluating soil-root inter- action of hybrid larch seedlings planted under soil compaction and nitrogen loading. *Forests* 11:1–14. https:// doi. org/ 10. 3390/ f1109 0947

Suvinen, A. (2006). A GIS-based simulation model for terrain tractability. *Journal of Terramechanics*. 43:427–449

Tarboron, D. G. (1997). A new method for the determination of flow directions and upslope areas in grid digital elevation models. *Water Resources Research*. *33*(2), 309–319. https://doi.org/10.1029/96WR03137

Toivio, J., Helmisaari, H-S., Palviainen, M., Lindeman, H., Ala- Ilomäki, J,, Sirén, M,, et al. (2017). Impacts of timber forwarding on physical properties of forest soils in southern Finland. *Forest Ecology and Management*. 405:22–30.

Weiss, a. (2001). Topographic position and landforms analysis. Poster Presentation, ESRI User Conference, San Diego, CA, *64*, 227–245. http://scholar.google.com/scholar?hl=en&btnG=Search&q=intitle:Topographic+Position+and+Landforms+Analysis#0

Zimmerman, J. L. and Shallenberger, J. P. (2016). GIS Topographic Wetness Index TWI Exercise Steps. *Susquehanna River Basin Commission*. https://www.chesapeakeconservancy.org/wp-content/uploads/2018/12/TWI-Work-Flow-Final.pdf